Stretch flow of thin layers of Newtonian liquids: Fingering patterns and lifting forces

A. Lindner
PMMH, Ecole Supérieure de Physique et de Chimie Industrielles, 10, rue Vauquelin, 75231 Paris Cedex 05, France

D. Derks
Soft Condensed Matter, Debye Institute, Utrecht University, Princetonplein 5, 3584 CC Utrecht, The Netherlands

M. J. Shelley[a)]
Applied Math Lab, Courant Institute, New York University, New York City, New York 10012

(Received 15 March 2005; accepted 3 May 2005; published online 13 July 2005)

We study the stretch flow of a thin layer of Newtonian liquid constrained between two circular plates. The evolution of the interface of the originally circular bubble is studied when lifting one of the plates at a constant velocity and the observed pattern is related to the measured lifting force. By comparing experimental results to numerical simulations using a Darcy's law model we can account for the fully nonlinear evolution of the observed fingering pattern. One observes an initial destabilization of the interface by growth of air fingers due to a Saffman–Taylor-like instability and then a coarsening of the pattern toward a circular interface until complete debonding of the two plates occurs. Numerical simulations reveal that when relating the observed patterns to the lifting force not only the number of fingers but also the amplitude of the fingering growth has to be taken into account. This is consistent with the experimental observations. © *2005 American Institute of Physics*. [DOI: 10.1063/1.1939927]

I. INTRODUCTION

The debonding of adhesively bonded surfaces occurs in a large number of situations, such as in food processing, in applications using pressure sensitive adhesives, and in biology (for example, the climbing of Geckos or insects).[1,2] The adhesive performance of these systems depends strongly on the details of the debonding mechanism. In particular, one often observes the formation of air fingers growing into the bulk adhesive, accelerating the debonding process. It is thus of great interest to be able to link adhesive performance directly to the formation of such structures. This requires a characterization of the observed pattern, and its relation to the material properties of the adhesive and the particular geometry of the system.

In the context of commercial adhesives, adhesive performance is typically tested with a so-called probe test:[3,4] A flat probe is brought into contact with the adhesive substrate and is then removed at a constant velocity. During the debonding one measures the lifting force as a function of the displacement of the probe. The force-displacement curves so obtained characterize the adhesive layer under tension and its form is determined by the microscopic debonding mechanism. The debonding occurs by the entry of air between the two debonding surfaces: the air can enter from the edges either through propagation of a crack between the adhesive and the surface or by penetration of air fingers into the bulk of the adhesive layer. In addition, cavitation in the bulk of the adhesive is often observed at the start of the debonding process. Propagation of cracks or fingers can also initiate at such internal defects.[5] In summary, the debonding mechanism is complicated to understand, and the force-displacement curves difficult to interpret, since different physical mechanisms can be simultaneously at play.[6]

The debonding of a number of other visco-elastic materials, such as clays, gels or paints, and the patterns that subsequently form during these stretch-flows, have also been studied both experimentally and theoretically.[7–12] However, due to the complexity of the visco-elastic materials used it remains difficult to predict the fingering patterns and little information is available about the relation between the observed patterns and the force-displacement relation.

Recently, purely elastic films[13] or viscous fluids have also been tested[10,11,14–17] and studied theoretically.[17] For Newtonian fluids the lifting force has been related to both cavitation and fingering. However, even for these simple fluids a large number of open questions remain. While it seems clear that the initiation of the fingering pattern observed is closely linked to the Saffman–Taylor instability,[10,11] the fully nonlinear growth mechanism of the fingering pattern has not yet been described and experiments attempting to link fingering patterns to lifting force are in disagreement.[10,14]

Here we compare experimental observations of the debonding of a Newtonian fluid with the results of direct numerical simulation of a Darcy's law model of the experiment. In the experiment, a Newtonian fluid is constrained by two closely spaced, parallel plates and one of the plates is lifted at a constant velocity. This leads to a debonding of the

[a)]Author to whom correspondence should be addressed. Electronic mail: shelley@cims.nyu.edu

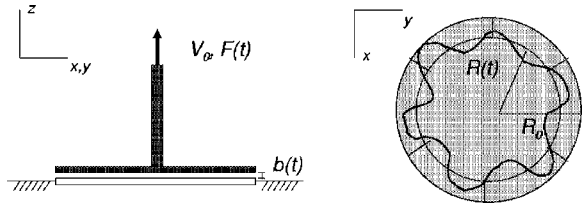

FIG. 1. Experimental setup: side view (left) and top view (right). A thin film of Newtonian liquid is confined between two circular plates. The upper plate is subsequently lifted at a constant speed V_0. b_0 is defined as the initial plate spacing and R_0 is the plate radius. $b(t)$ and $R(t)$ denote the evolution of the latter with time. The lifting force is measured during the lifting of the upper plate and the evolution of the air–fluid interface is captured with a CCD camera through the glass plate at the bottom.

two surfaces as air fingers enter into the fluid from the outside. These fingers develop initially in the nearly circular interface through a version of the Saffman–Taylor instability that accounts for the change in plate spacing. The fully nonlinear evolution ultimately shows a coarsening of the fingering pattern and finally a contraction of the interface back to a circular interface. Coarsening dynamics have recently been studied in relaxing (unforced) bubbles in Hele-Shaw cells.[18,19] The lifting force is measured simultaneously with the observation of the fingering pattern. The comparison of these data with those of the fully nonlinear numerical simulations of the bubble dynamics has given us a much more refined understanding of the relation between the evolution of the liquid bubble and the lifting force.

This paper is organized as follows. In Secs. II and III we give the model equations and discuss our experimental and numerical methods. In Sec. IV we discuss the fingering patterns, comparing results from experiments and numerical simulations. These results will then be used to discuss the lifting force in Sec. V, comparing again experimental data to numerical simulations. Finally in Sec. VI we present our conclusions.

II. MODEL EQUATIONS

We study here a bubble of Newtonian fluid with viscosity η and surface tension σ and confined between two parallel plates separated by a small gap of time-dependent width $b(t)$ (see Fig. 1). Denote the bubble cross-section in the (x,y)-plane (of the plates) by $\Omega(t)$ and its time-dependent boundary by $\Gamma(t)$. Following Shelley *et al.*[20] we model the evolution of this system using Darcy's law for Hele-Shaw flow in a time-dependent gap:

$$\begin{aligned}
&\mathbf{u}(x,y,t) = -\frac{b^2}{12\eta}\nabla p(x,y,t) \quad \text{in } \Omega(t),\\
&\nabla\cdot\mathbf{u} = -\frac{\dot{b}(t)}{b(t)} \quad \text{in } \Omega(t),\\
&p = \sigma\kappa \quad \text{on } \Gamma(t),\\
&u_n = -\frac{b^2}{12\eta}\frac{\partial p}{\partial n} \quad \text{on } \Gamma(t).
\end{aligned} \tag{1}$$

The PDEs (partial differential equations) for the velocity $\mathbf{u}$ and pressure p in Ω can be derived directly from the Navier–Stokes equations using $\epsilon = b_0/L_0$ as a small parameter, where L_0 is a characteristic scale of the initial bubble. It must be assumed that the aspect ratio of the system remains small. The leading order system is a reduced Stokes equation where lateral pressure gradients balance gap-wise (second) derivatives of lateral velocities, with a constant gap-wise pressure. Gap-averaging these reduced equations, as well as the three-dimensional divergence free condition on velocity, leads directly to the above system. Hence $\mathbf{u}$ is the gap-averaged fluid velocity. In the boundary conditions, κ is the curvature of $\Gamma(t)$ which has normal velocity u_n. Once the initial boundary position Γ_0 is given then the evolution of the system is completely specified. Following previous analyses, we have not included within the pressure boundary condition the contribution from the meniscus curvature across the gap.[21–24] While that contribution is large $[O(b^{-1})]$ it is uniform along the interface and so does not contribute to the dynamics or the force measurements (i.e., it can be absorbed into an overall constant pressure background).

A. Fingering

Consider a perfectly circular bubble of initial radius R_0, and with the upper plate being lifted at constant velocity V_0, i.e., $b(t) = b_0 + V_0 t$. This leads to a contraction of the circular bubble of fluid with inward velocity U at the moving interface (corresponding to u_n). Due to the conservation of the total volume of fluid $\Lambda = \pi R_0^2 b_0$, the bubble radius is given by $R(t) = R_0\sqrt{b_0/b(t)}$, and $U(t) = -V_0 R(t)/2b(t)$.

However, as the bubble contracts the circular interface destabilizes and perturbations can lead to the formation of fingers, similar to those observed in the Saffman–Taylor instability. Shelley *et al.*[20] analyzed this instability in the dynamics of Eq. (1) linearized about the contracting circular interface. Applying their general result to a plate lifting with constant speed V_0, they show that for sufficiently fast lifting, or sufficiently small surface tension, there exists a band of unstable azimuthal modes whose wave-numbers n satisfy

$$2 \leqslant |n| < \sqrt{1 + \frac{1}{2\tau(1+t')^{9/2}}} \tag{2}$$

and where maximal growth occurs at the wave-number

$$n_{\max} = \sqrt{\frac{1}{3}\left(1 + \frac{1}{2\tau(1+t')^{9/2}}\right)}. \tag{3}$$

Here $t' = t(V_0/b_0)$ is a dimensionless time, and $\tau = \sigma(b_0^3/12V_0\eta R_0^3)$ a dimensionless surface tension. This instability is the Saffman–Taylor instability for the lifting plate system. An important element of this particular instability (unlike the related sink driven instability analyzed by Paterson[25]) is that when t' is large enough the band of unstable modes is lost and the (shrinking) circular bubble becomes stable again.

Scaling time as above, x and y by the initial radius R_0, and pressure by $12\eta R_0^2 V_0/b_0^3$, gives the dimensionless form of Eq. (1):

$$\mathbf{u} = -b^2 \nabla p \quad \text{and} \quad \nabla \cdot \mathbf{u} = -\dot{b}/b \quad \text{in } \Omega,$$
$$p = \tau\kappa \quad \text{and} \quad u_n = -b^2 \frac{\partial p}{\partial n} \quad \text{on } \Gamma, \tag{4}$$

where the initial data now have unit characteristic scale, and for the experiments and simulations discussed here, $b=1+t'$ and $\dot{b}=1$. Hence τ is the single control parameter. To avoid excessive notation, we have used the same variables for adimensional as for dimensional ones, with the exception of the adimensional time t'. Unless otherwise stated, henceforth we shall only be dealing with dimensionless quantities.

B. The lifting force

We estimate the force required to lift the plate at a given rate by integrating the pressure stress over the bubble area:

$$F(t') = \int_{\Omega(t')} (-p) dA. \tag{5}$$

Using Eq. (4), we can express this force as a boundary plus a bulk contribution. Letting $\mathbf{x}=(x,y)$ and $m_2=\mathbf{x}\cdot\mathbf{x}/2$, then $\nabla m_2=\mathbf{x}$ and $\Delta m_2=2$. Representing the boundary Γ by $\mathbf{X}(s)$ where s is arclength, and with outward normal $\hat{\mathbf{n}}$, we have the string of identities:

$$\begin{aligned} F &= -\int_{\Omega(t')} p(\mathbf{x},t') dA = -\frac{1}{2}\int_{\Omega(t')} p\ \Delta m_2 dA \\ &= -\frac{1}{2}\int_{\Omega(t')} [\nabla\cdot(p\nabla m_2) - \nabla p\cdot\nabla m_2] dA \\ &= -\frac{1}{2}\int_{\Gamma(t')} \tau\kappa\hat{\mathbf{n}}\cdot\mathbf{X}\ ds - \frac{1}{2b^2}\int_{\Omega(t')} \mathbf{u}\cdot\mathbf{x}\ dA \\ &= F_{\text{cap}} + F_v, \end{aligned} \tag{6}$$

where we have used the divergence theorem and the boundary condition on p. Both terms can be considerably simplified. Using the Frenet–Seret formula $\mathbf{X}_{ss}=-\kappa\hat{\mathbf{n}}$ (subscript s denotes a partial derivative), and integrating the first integral by parts, gives directly

$$F_{\text{cap}}(t') = -\frac{\tau}{2}\int_{\Gamma(t')} \mathbf{X}_s\cdot\mathbf{X}_s ds = -\frac{\tau L(t')}{2}, \tag{7}$$

where L is the length of the bubble perimeter. To treat the second integral, we introduce the Lagrangian coordinate $\mathbf{x}_0$ of the two-dimensional flow in $\Omega(t')$, that is, $(\partial/\partial t')\mathbf{X}(\mathbf{x}_0,t')=\mathbf{u}(\mathbf{X}(\mathbf{x}_0,t'),t')$ with $\mathbf{X}(\mathbf{x}_0,0)=\mathbf{x}_0$. Let $J=\det[\partial\mathbf{X}/\partial\mathbf{x}_0]$ be the Jacobian of this flow map. One can show that $(\partial/\partial t')(bJ)=0$, which is an expression of three-dimensional conservation of volume. By changing to Lagrangian variables, and multiplying and dividing by b, we can rewrite the second integral as

$$\begin{aligned} F_v(t') &= -\frac{1}{2b^3}\int_{\Omega(0)} \mathbf{X}_{t'}\cdot\mathbf{X}(bJ) dA \\ &= -\frac{1}{2b^3}\frac{d}{dt'}\left[b\int_{\Omega(t')} m_2 dA \right] \\ &= -\frac{1}{2b^3}\frac{d}{dt'}[b(t')M_2(t')], \end{aligned} \tag{8}$$

where $M_2(t')=\int_{\Omega(t')} m_2 dA$ is the (unnormalized) second moment of the fluid domain $\Omega(t')$.

In dimensional form, the lifting force is

$$F(t) = -\frac{\sigma L(t)}{2} - \frac{6\eta}{b^3}\frac{d}{dt}[b(t)M_2(t)], \tag{9}$$

and is thus expressed naturally as a boundary contribution proportional to surface tension, plus a bulk contribution due to the Poiseille flow and proportional to viscosity. We find in all cases considered here that F_{cap} is much smaller than F_v, and henceforth we will concentrate on this latter quantity.

When assuming a circular interface during the contraction of the bubble by a plate lifting with constant speed V_0, the dimensional viscous lifting force is given by

$$F_v(t) = \frac{3\eta\Lambda^2 V_0}{2\pi b^5(t)}, \tag{10}$$

which is used extensively in Derks *et al.*[10] The dimensionless form is simply

$$F_v(t') = \frac{\pi/8}{b^5(t')} = \frac{\pi/8}{(1+t')^5}. \tag{11}$$

III. METHODS

A. Simulational methods

For the purposes of simulating the dynamics of the contracting bubble, Eq. (4) can be reformulated using boundary integral methods, which is the basis for our simulations here, as in Shelley *et al.*[20] This reformulation reduces the dynamics of the bubble to the evolution of its interface Γ, expressed completely in terms of interfacial quantities. Our simulations are of infinite-order accuracy in space and second-order accurate in time. Generally we use 4096 points, equally spaced in arclength, to describe the interface. In particular, for the initial data used here there are never fewer than 50 points per wavelength. Below $\tau\approx 5\times 10^{-5}$, we find that this resolution is insufficient, and the simulations becomes unstable. To remove high-order stability constraints arising from the curvature forces we employ the "small-scale decomposition" method of Hou, Lowengrub, and Shelley.[26,27] This allows us to efficiently evolve the system to long times. There does remain a first-order Courant–Friedrichs–Levy constraint on the time-step, which is satisfied by automatic readjustment of the time-step when necessary.

B. Experimental methods

The experimental setup (see Fig. 1) consists of a thin layer of a Newtonian fluid confined between two parallel circular plates. The upper plate can be lifted at constant velocity V_0 leading to a contraction of the circular air–fluid interface and finally to debonding of the two surfaces. During this process the interface is destabilized leading to the formation of fingers. The evolution of the pattern is observed during the experiment and the lifting force is measured as a function of the distance of the two plates.

For our experiments we use the plate–plate geometry of a Rheologica StressTech rheometer equipped with a normal force transducer. The driving velocity V_0 can be varied and the exact value imposed by the apparatus is measured during the experiments. For the experiments presented here we mostly used $V_0=0.73\pm0.05$ μm/s and more rarely $V_0=8.73\pm0.05$ μm/s. The plate radius is $R_0=20$ mm. The upper plate is made of metal, whereas the lower is of glass, allowing for the observation (and video recording via CCD camera) of the evolution of the air–fluid interface during the debonding process. The initial thickness of the layer b_0 is typically between 0.1 mm and 0.4 mm. The lifting force is measured with an accuracy of 0.04 N and the plate separation distance with an accuracy of 1 μm. Both are read out directly using a data acquisition card and yield force-distance curves.

For the fluid we use a silicon oil (polydimethylsiloxane, PDMS 200 fluid, from Aldrich) of viscosity $\eta=92$ Pas. Other silicon oils ($\eta=11.5$ Pas and $\eta=28.5$ Pas) have also been used. Occasionally we will refer to these experiments. The viscosities of the silicon oils have been measured on the Rheologiga StressTech rheometer at $T=22$ °C, corresponding to the temperature of the debonding experiments. Note that for the low shear rates observed in our experiments ($\dot{\gamma}<1$ s^{-1}) the silicon oils behave as purely Newtonian fluids. The surface tension of these silicon oils is, as given by Aldrich, $\sigma=20$ mN/m.

Special care is taken when confining the fluid between the two plates. First a given amount of fluid is applied to the lower plate. The upper plate is then slowly lowered until the desired gap width is reached. The excess oil is carefully removed from around the plates and before starting the experiment one waits until complete relaxation of the fluid, which means that the normal force has dropped to zero. Still, we never wait too long before beginning an experiment to avoid flow of the silicon oil, even if the high viscosities and the high confinement make this process very slow.

In summary, the experimental setup allows us to study the evolution of the air–fluid interface by analyzing the video images. The pattern can be characterized by measuring the number of fingers as a function of time and, for example, the length of the interface. The setup allows us to also obtain the force-distance curves, which can then be related to the observed patterns.

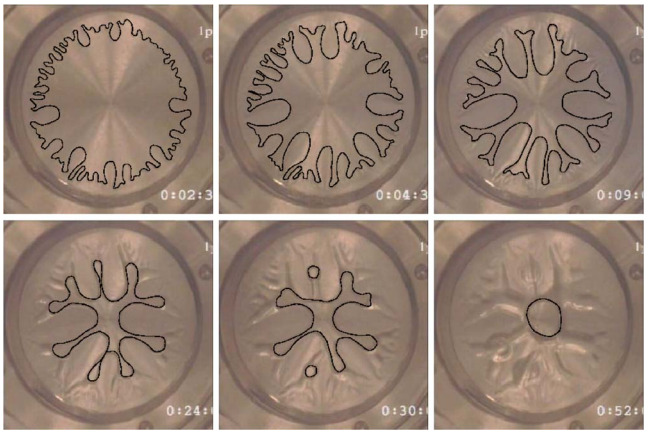

FIG. 2. Snapshots of experimental evolution of the fingering pattern. This example is for a silicon oil of viscosity $\eta=92$ Pas and initial plate spacing $b_0=0.2$ mm leading to a control parameter of $\tau=2.5\times10^{-5}$. The snapshots are taken at times $t'=0.5$, 1, 2, 5.3, 6.6, 11.4. The squares shown in Fig. 4 correspond to this experiment.

IV. CHARACTERIZING THE FINGERING PATTERNS

A. Qualitative observations

When comparing the evolution of the experimentally observed patterns (Fig. 2) and the results from the simulations (Fig. 3) it is clear that they are qualitatively very similar. In both cases the circular interface destabilizes and at early times a large number of fingers develop. While the amplitude of these fingers grows in time, their number decreases. We observe a coarsening of the pattern that leads eventually to a retraction to a nearly circular shape (though not shown for the simulations here; see Shelley *et al.*[20]). In the experiment, the splitting off of droplets from the main bubble body can be observed. In the simulations, there are instances of near collision of the interface (see the lower left panel of Fig. 3), but apparently no true ones. One aspect of the mathematical model is that it does not incorporate the geometric effect of the meniscus curvature across the gap, which yields an effective "cross-interface" width. Further, being fundamentally a "sharp interface" model, it contains no mechanism for evolving through such an event. Still, collisional singularities have been found and studied in Hele-Shaw flows modeled by Darcy's law,[28] and we cannot discount their possibility here.

B. Number of fingers and perimeter length

1. From experiment

We now characterize the experimentally observed patterns in more detail. The linear theory of Sec. II [i.e., Eq. (3)] suggests that the number of fingers depends only on τ and one might then expect that the evolution of the pattern, as a function of dimensionless time t', is also determined by τ. Thus we study a set of experiments using the same silicon oil ($\eta=92$ Pas), but varying the initial plate spacing b_0. All other parameters remain unchanged ($R_0=20$ mm and $V_0=0.73$ μm/s). We use three different plate spacings: $b_0=0.2$ mm, 0.3 mm, and 0.4 mm, leading to $\tau=2.5\times10^{-5}$, 8.4×10^{-5}, and 2×10^{-4} as values for the dimensionless surface tension, respectively.

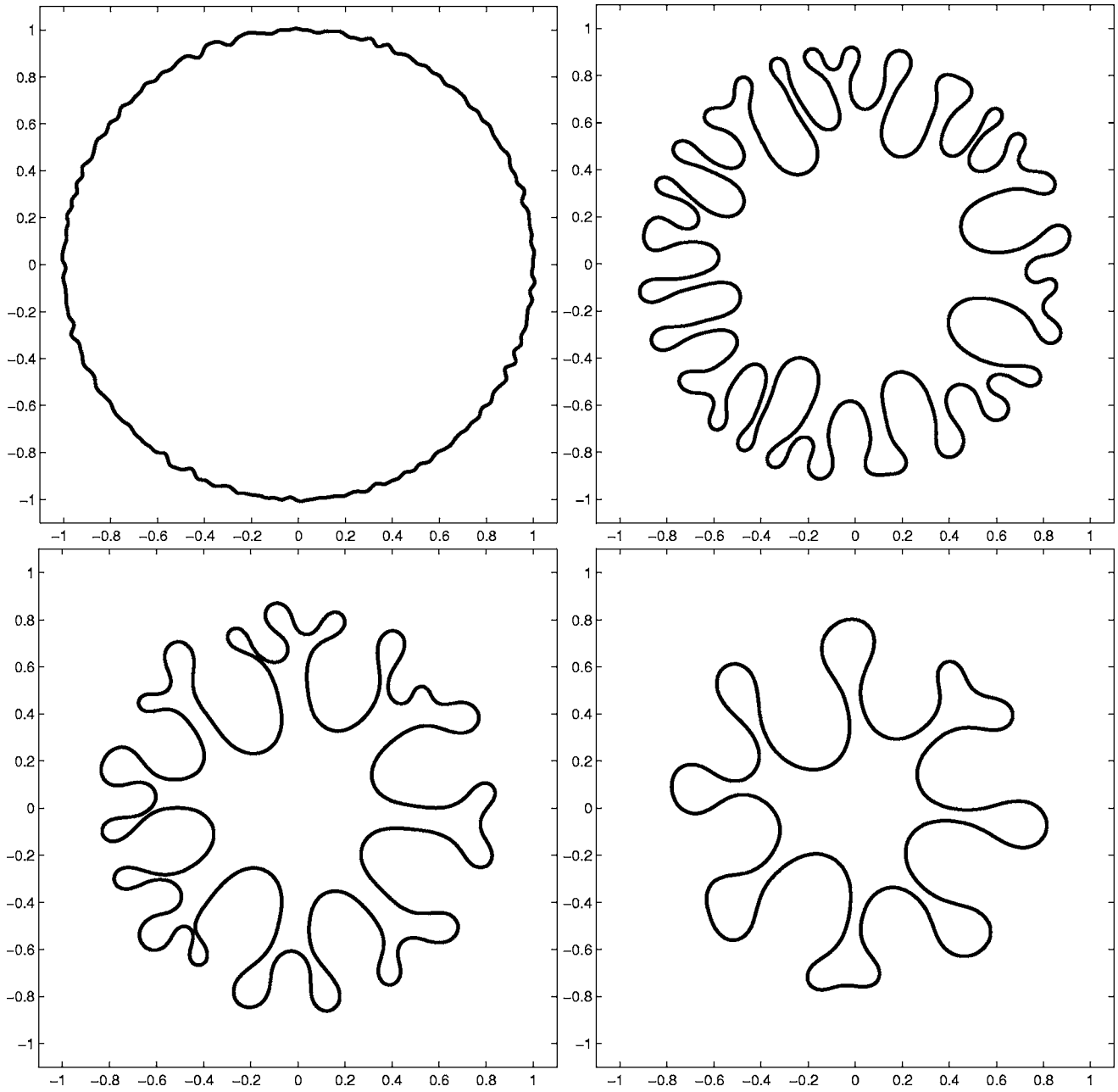

FIG. 3. From simulation, the evolution of fingering patterns with $\tau=5\times10^{-5}$ and shown at times $t'=0$, 1, 2, and 3.

One dominant feature that characterizes the observed pattern is the formation of fingers, and we show their number in Fig. 4 as a function of the dimensionless time for the three different dimensionless surface tensions. For each surface tension, three to four experimental runs were performed and are represented in the graph. Some scatter of the data is noticeable, being mainly due to the fact that it is not always evident how to count the number of fingers, especially when the growth of the fingers is not very pronounced. This is the case for the experiment with the highest surface tension, where one observes a small number of fingers, leading to stronger scattering of the data as can be seen from the figure. This uncertainty in counting makes it also difficult to obtain the number of fingers very early in the experiments before significant growth has set in. Further, the time $t'=0$ is not perfectly well defined as the synchronization between the rheometer and the video recording is done by hand. Furthermore, there might be a short delay before the upper plate of the rheometer starts to move.[16] This error is, however, small and the maximum possible time shift for this set of experiments can be estimated as $\Delta t'=0.1$. This should mainly be important for the lowest surface tension, where the variation of the number of fingers as a function of t' is strong in the beginning of the experiments. In summary, the highest experimental confidence is reached for the experiments for $\tau=8.4\times10^{-5}$. But even if there is some experimental error, the different experimental runs scale reasonably well and it can be concluded that the number of fingers decreases as a function of time (as could already be seen from the snapshots

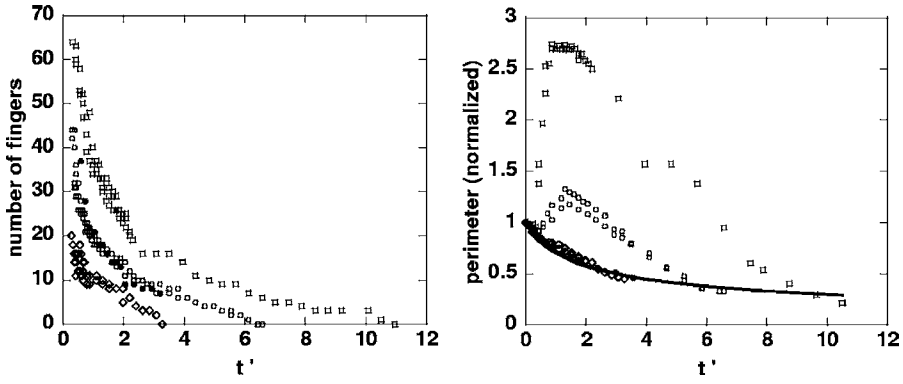

FIG. 4. The figure shows experiments for the same silicon oil (η=92 Pas), but different initial plate spacings b_0 =0.2 mm (□), b_0=0.3 mm (◯), and b_0=0.4 mm (◇), leading to $\tau=2.5\times10^{-5}, 8.4\times10^{-5}$, and 2.0×10^{-4}, respectively. (Left) The number of fingers as a function of t'. (Right) Evolution of the perimeter as a function of $t'=t(V_0/b_0)$. The solid line represents the evolution of a circular interface.

shown in Fig. 2). It is also evident that, as expected, the number of fingers increases when using lower surface tensions.

To check whether the evolution as a function of t' is really only controlled by the value of τ we have reproduced the dimensionless surface tension of $\tau=8.4\times10^{-5}$ for another experimental condition, by using a different silicon oil of lower viscosity η=11.5 Pas and changing the initial plate spacing to b_0=0.15 mm. The lifting velocity V_0 and the radius R_0 of the plates remain unchanged. The results are shown in Fig. 5 (closed symbols). One concludes that the data scale very well, with τ organizing the data. Note that other experiments (not shown here) have also been performed for a higher lifting velocity. When scaled on the dimensionless time these results also fit well as a function of the control parameter into the results shown in Fig. 4.

In summary one can conclude that the evolution of the number of fingers as a function of t' is determined by the dimensionless surface tension τ, which is thus effectively the sole control parameter for our system. Thus far we have not discussed the exact evolution of the number of fingers as a function of time. This will be done when comparing the experimental results to the numerical simulations. However, Eq. (3) of the linear stability analysis does suggest already that the number of fingers decreases as the upper plate is lifted. While linear theory does not adequately account for the fully nonlinear evolution, the experiments show a qualitative conformance to its predictions discussed in Sec. II A: The increase of plate spacing leads to bubble contraction and a lower velocity of the advancing interface. This means that the surface tension forces become increasingly dominant, reducing the number of fingers and finally yielding a contraction toward a circular interface. However, as will be discussed in detail below, we do note that the evolution of the number of fingers as a function of time is not following a power law as given by the estimate of Eq. (3) for $n_{\max}(t)$ from linear stability analysis, but rather appears to be nearly exponential.

Another important characteristic of the observed pattern is the extent of finger growth. It will be shown below that it is precisely this characteristic of the patterns that governs the influence on the lifting force. One measure of this is the perimeter length $L(t)$ of the dynamic pattern, which we measure by image processing. This is shown in Fig. 4 (right) for the set of experiments described above, where we have scaled the initial perimeter to be unity. Initially the evolution of the perimeter length is close to that of a circular interface, but as fingering sets in the length grows strongly. At later times the perimeter length begins to decrease and one observes relaxation toward a contracting circle. We see less pronounced fingering when increasing the initial plate spacing while keeping the other parameters constant. For this set of experiments the deviation from the evolution of a circular

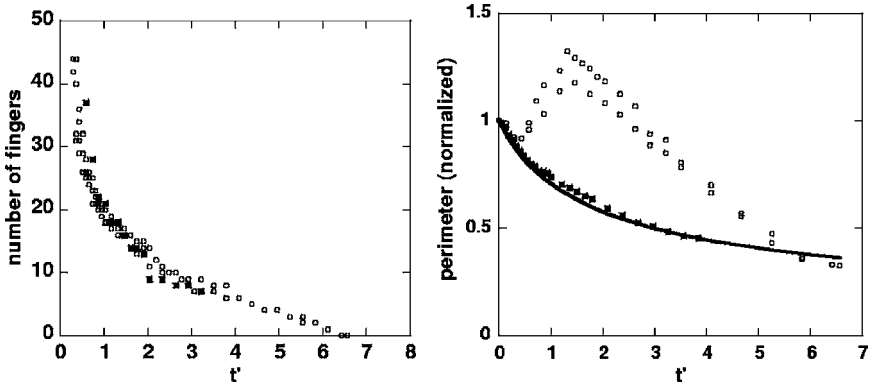

FIG. 5. The figure compares experiments for the same control parameter $\tau=8.4\times10^{-5}$ but two different experimental conditions. In particular the experiments have been performed using two different silicon oils and different initial plate spacings b_0 while the plate radius R_0 and the lifting velocity V_0 are kept constant. The open symbols correspond to the experiment already shown in Fig. 4 and thus to an initial plate spacing b_0=0.3 mm and η=92 Pas. The closed symbols correspond to an initial plate spacing of b_0=0.15 mm and η=11.5 Pas. (Left) Number of fingers as a function of t'. (Right) Evolution of the perimeter as a function of $t'=t(V_0/b_0)$, for the same experiments as shown on the left side. The solid line represents the evolution of a circular interface.

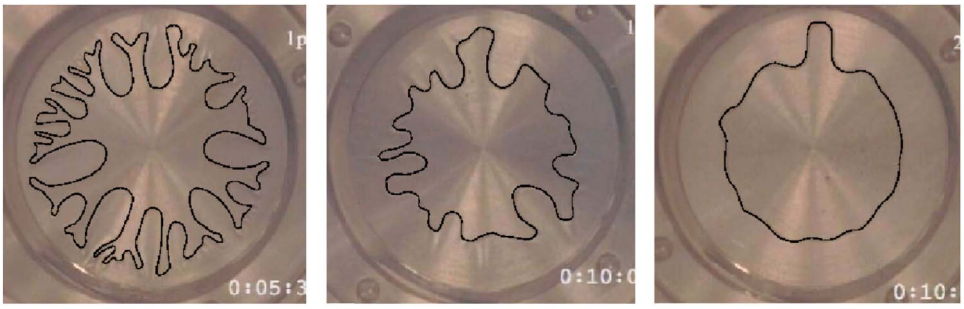

FIG. 6. Snapshots of the experimentally observed fingering patterns for different surface tensions: $\tau=2.5\times10^{-5}$, 8.4×10^{-5}, and 2×10^{-4} from left to right. The images are always taken at the time t' that corresponds to the maximal extent of finger growth and thus to the maximum of the perimeter length shown on Fig. 4 (right).

interface is thus most pronounced for the smallest surface tension, where the number of fingers is also the highest. This is also illustrated by Fig. 6 showing snapshots of the observed fingering patterns for the different control parameters. The images are always taken at the time t' corresponding to the maximal extent of finger growth and thus the maximum of the perimeter length shown in Fig. 4. Also, the results for different experiments performed under the same experimental conditions generally collapse onto a single curve. The experimental error can be estimated from the scatter of the data obtained from different experimental runs. However, in some cases one does observe the predominant growth of a single distinguished finger, which for runs for the same experimental conditions can lead to quite different evolutions.

We now discuss what happens to the perimeter length when one changes the experimental conditions but keeping the same control parameter. These results are shown in the right panel of Fig. 5 (same two experiments as in the left panel). The observation is unlike that for the number of fingers; one now observes a very different evolution of the perimeter length for these two cases, with the experiment with lower initial plate spacing showing much less pronounced finger growth. Our interpretation is that the amount of growth of the observed fingers (i.e., perimeter length growth) is not solely a function of the control parameter, but also depends strongly on initial conditions, which are different in the two experimental situations. These initial conditions, like the different initial plate spacings or even the way the sample has been prepared by removing the excess oil from around the plates, could have an influence on the air–oil interface at the beginning of the experiments. We shall discuss below whether this is consistent with our simulational results.

Figure 7 shows snapshots at the same dimensionless time for the two different experiments of $\tau=8.4\times10^{-5}$. At the top is the experiment with $b_0=0.3$ mm and $\eta=92$ Pas (A) and at the bottom that with $b_0=0.15$ mm and $\eta=11.5$ Pas (B). The number of fingers is roughly the same for both experiments though the fingering is much more pronounced for the larger gap-width $b_0=0.3$ mm. This comparison nicely illustrates that the number of fingers is a relatively robust parameter determined by the dimensionless surface tension only, while the growth of perimeter length is less robust and likely to depend strongly upon initial conditions. This suggests that differing protocols for preparing the air–fluid interface at the beginning of the experiment can lead to very different finger growth, but roughly the same number of fingers.

2. From simulations

We have simulated the pattern formation for many sets of initial data, varying the form of the initial data, such as its modal content, as well as amplitude. To be specific in our comparison with experiment, we fix $\tau=8.4\times10^{-5}$, and consider the results of some of these simulations. First we note that for this value of τ, linear theory predicts that at $t'=0$ the azimuthal mode of maximum growth, $n_{\max}$, is approximately 45, with $n\in[2,\bar{n}\approx77]$ being the band of unstable modes [using Eqs. (2) and (3)]. The dark dashed lines in Fig. 9(a) show the decrease in $n_{\max}$ (lower) and $\bar{n}$ (upper) as functions of time, while the dark dashed line in Fig. 9(b) shows the (normalized) perimeter length of the exact solution of a contracting circle. For the simulations, we will define the num-

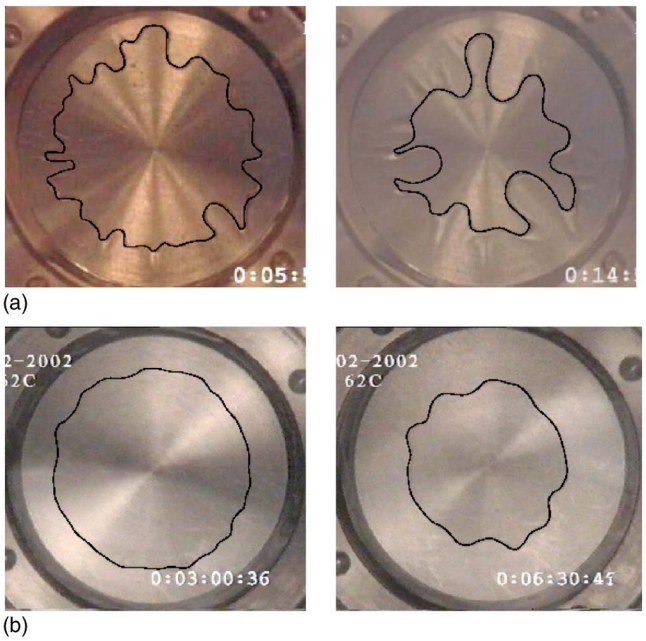

FIG. 7. Snapshots of two experiments (as shown in Fig. 5) for the same control parameter $\tau=8.4\times10^{-5}$ but different experimental conditions. (Top) $\eta=92$ Pas and $b_0=0.3$ mm. (Bottom) $\eta=11.5$ Pas and $b_0=0.15$ mm. The snapshots on the left are taken at $t'=0.88$ and the snapshots on the right at $t'=2.19$.

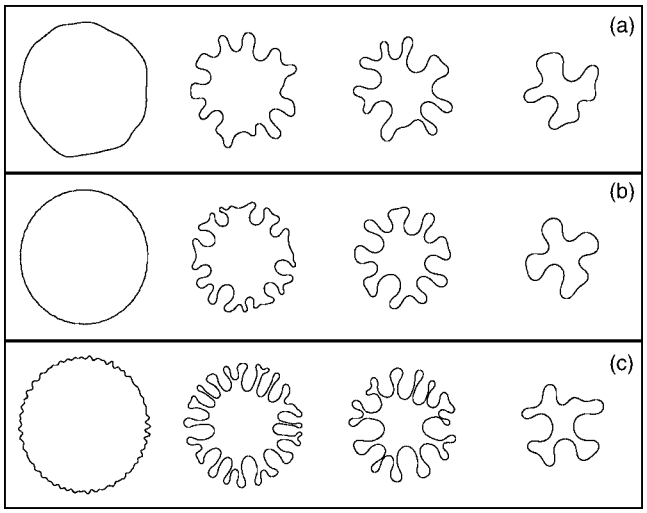

FIG. 8. For $\tau=8.4\times10^{-5}$ the simulated evolution from of the liquid bubble for three different types of initial data, each close to circular, as the perturbation amplitude and band of perturbed azimuthal modes are varied. Shown at times $t'=0$, 1, 2, and 4.

ber of fingers in the simulation as the number of minima in the distance function of the interface position from the origin.

Figure 8 shows the results of three simulations, each evolving from nearly circular initial data of the form

$$[x_0(\theta),y_0(\theta)]=r(\theta)(\cos\theta,\sin\theta),$$

$$r(\theta)=1+\epsilon\sum_{k=k_{\min}}^{k_{\max}}e^{-\alpha k}[a_k\cos k(\theta-\phi_k)+b_k\sin k(\theta-\psi_k)]. \tag{12}$$

Here, for each k, a_k and b_k are chosen uniformly on $(-1,1)$, and ϕ_k and ψ_k are chosen uniformly on $(0,2\pi)$. Varying $\epsilon,\alpha,k_{\min}$, and $k_{\max}$ allows us to vary the amplitude of the perturbation and its modal content. We briefly describe and compare these three simulations:

(i) For Fig. 8(a), $\epsilon=0.05$, $\alpha=0.2$, $k_{\min}=2$, and $k_{\max}=100$. While the range of initial wave-numbers is broad, these initial data are dominated by the low wave-numbers. This is carried over into the subsequent evolution where the low modes also dominate, leading to a relatively modest number of fingers shown as the "*" symbols in Fig. 9(a). The (normalized) perimeter length of this simulation is shown as the solid curve in Fig. 9(b).

(ii) For Fig. 8(b), $\epsilon=0.0025$, $\alpha=0.2$, $k_{\min}=30$, and $k_{\max}=60$. Here the initial perturbation is restricted to a band of high wave-numbers that includes the mode of maximal growth. Consequently, these modes dominate the subsequent evolution, which is particularly evident at intermediate times, as is seen in Fig. 9(a) ($\triangle$ symbols). This increased ramification of the interface is reflected also in the perimeter length [dashed curve in Fig. 9(b)]. Two other simulations were also performed for this set of parameters, using different random number seeds to generate the initial data. While the details of each evolution were different, the number of fingers developed in each simulation was roughly the same. This rough similarity for the three different simulations was also evident in the (normalized) perimeter length.

(iii) For Fig. 8(c), $\epsilon=0.02$, $\alpha=0.2$, $k_{\min}=30$, and $k_{\max}=60$. Here the perturbation amplitude is increased by a factor of 8. Relative to the previous cases, the in-rushing fingers are better developed, yielding a more organized pattern. The number of fingers developed is similar to that of the previous case [$\bigcirc$ symbols in Fig. 9(a)], but with deeper patterning as shown also by the perimeter length [dot-dashed curve in Fig. 9(b)]. As with case B, two other simulations were also per-

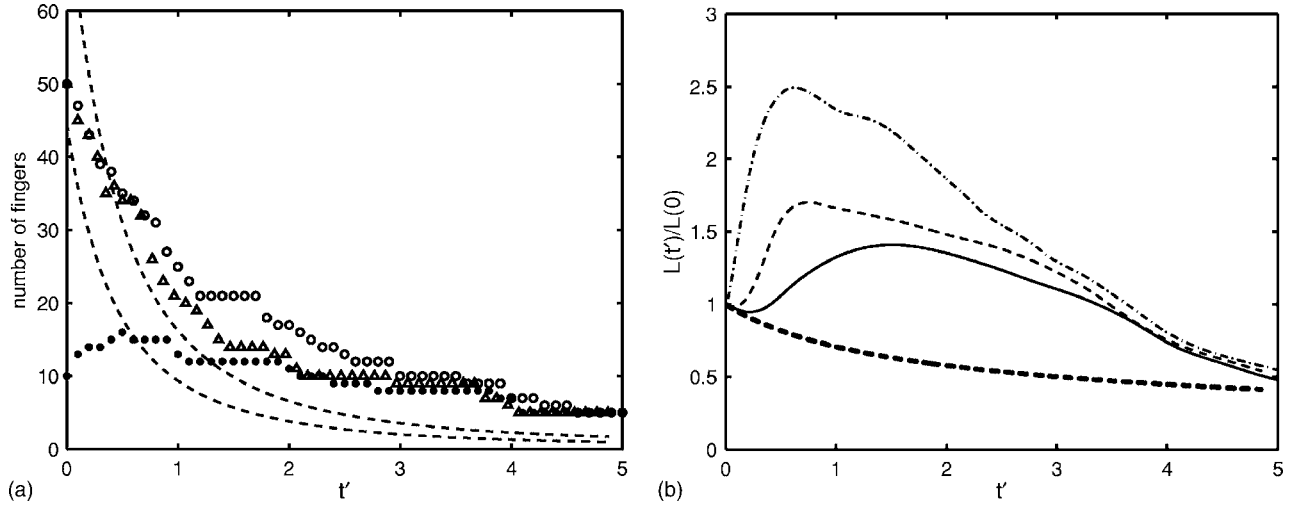

FIG. 9. (a): The number of fingers as a function of time for $\tau=8.4\times10^{-5}$ for the simulations shown in Fig. 8, i.e, for case A (●), case B ($\triangle$), and case C ($\bigcirc$). The lower dashed line shows the time evolution of the azimuthal wavenumber of maximal growth from linear theory [Eq. (3)], while the upper dashed curve shows the upper bound on the band of linearly unstable modes [Eq. (2)]. (b): The normalized perimeter length for the simulations of case A (solid), case B (dotted), and case C (dot-dashed). The dashed curve shows the perimeter length for the exact solution of a contracting circle.

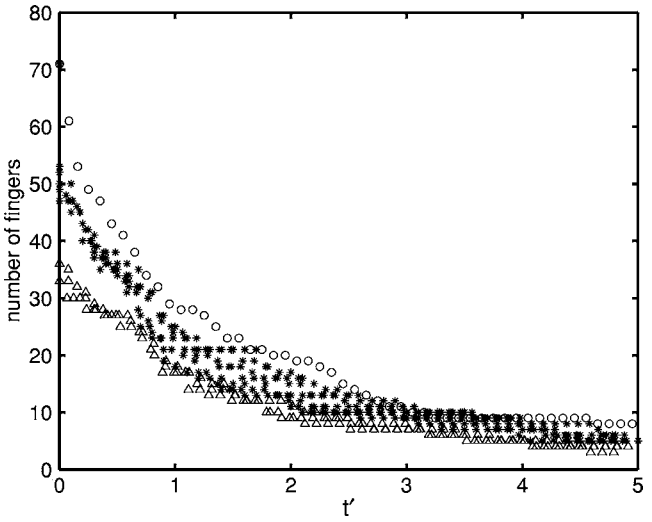

FIG. 10. A comparison of the number of fingers developed as the effective surface tension τ is varied for $\tau=2\times10^{-4}$ (△), $\tau=8.4\times10^{-5}$ (∗), and $\tau=5\times10^{-5}$ (○).

formed for the same parameters, but using different random number seeds. These again showed rough similarity in both the number of fingers developed and in perimeter length.

From Fig. 9(a) we see that at early times, the most unstable mode (lower dashed curve) does a reasonable job in predicting the initial number of fingers, though it is an underestimate. This underestimation by $n_{\max}$ is not surprising given that higher wave-number modes in its neighborhood have similar (though smaller) growth rates. Indeed, the subsequent evolution of the pattern is the steady coarsening of the pattern set in the early evolution. Figure 10 shows how the number of fingers produced depends upon the value of the effective surface tension τ. Here we are including results from the many different simulations (three for $\tau=2\times10^{-4}$, seven for $\tau=8.4\times10^{-5}$ excluding case A, and one simulation for $\tau=5\times10^{-5}$). As pointed out before it was not possible to run simulations for values of the surface tension τ below $\tau=5\times10^{-5}$. The smallest surface tension used in the experiments could thus not be compared with the simulations. Still, the results from the simulations are consistent with the experimental results, with decreases in τ yielding typically greater numbers of fingers. We also find that at a given τ the simulations produce roughly the same number of fingers, so long as a sufficiently broad band of high wave-numbers is initially excited.

In summary, we find that there is a complicated dependence of the characteristics of the pattern on the initial data. So long as a sufficiently large set of short wavelength modes are initially excited, then the number of fingers is robustly reproduced, though the perimeter lengths may vary significantly. Conversely, if longer wavelength modes are initially dominant then highly ramified patterns are not produced and the number of fingers is smaller than otherwise. Similarly, we have also found that if the amplitude of the initial perturbation is too small, that is the bubble initial data are too close to that of the circle, then the growth of fingers can be cut short by the restabilizing of the contracting bubble at later times.

3. Comparison of simulations and experiments

For $\tau=8.4\times10^{-5}$, Fig. 11(a) shows a comparison of the number of fingers counted in our simulations and in the experiments. The simulational results combine those of many different simulations where well-ramified patterns developed (six different simulations, omitting case A of Fig. 8), and the experimental results are for the two experiments shown in Fig. 5. It is clear from Fig. 11(a) that the overall agreement between simulation and experiment is very good. Figure 11(b) shows the same data on a log-linear scale. While the number of fingers counted spans only one decade at best, this plot does suggest a nearly exponential decrease, which is much different from the algebraic decay suggested by linear theory.

Another point of comparison is perimeter length. Figure 5 shows that those experiments that develop fingering patterns peak in their length growth at times slightly past $t'=1$,

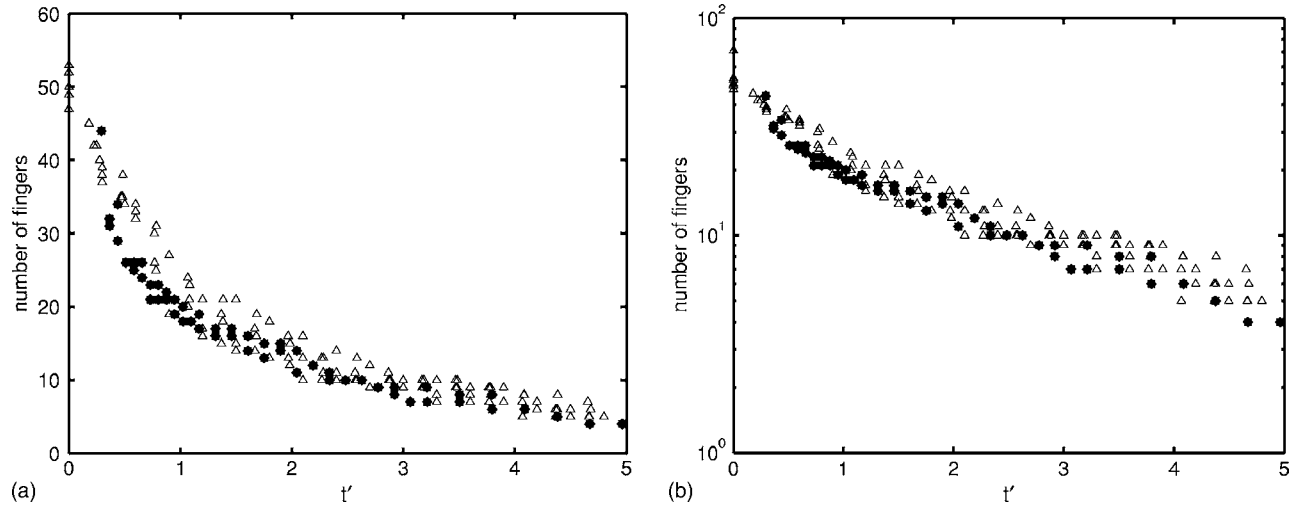

FIG. 11. (a) For $\tau=8.4\times10^{-5}$, the number of fingers measured in various simulations (△) and in experiments (∗). (b) The log-linear plot of these data.

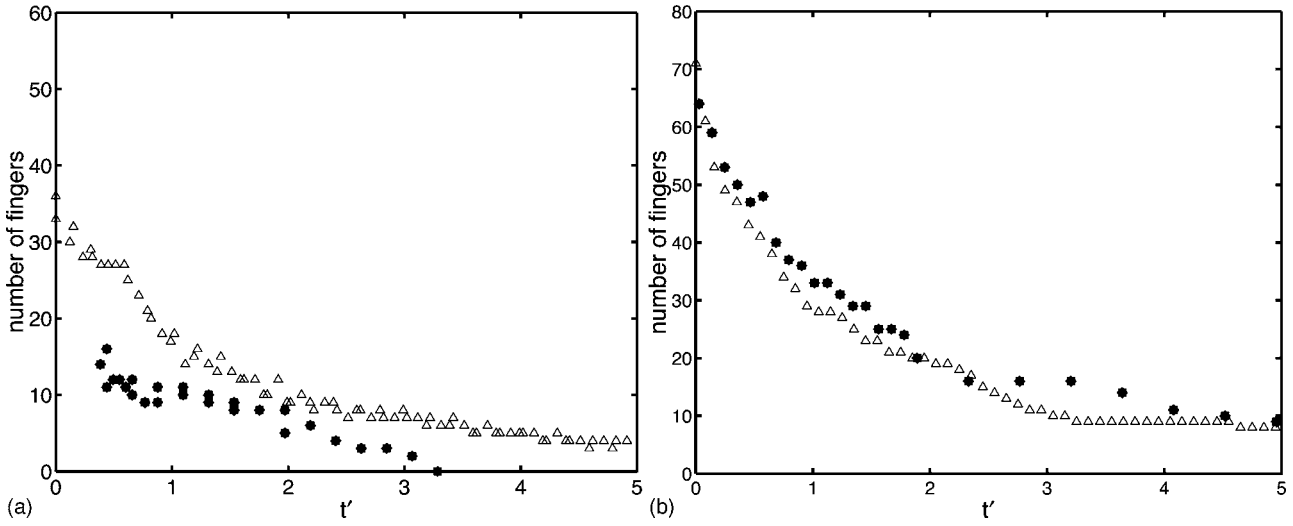

FIG. 12. A comparison of the number of fingers found in simulation (△) and from experiment (∗), for the values $\tau=2\times10^{-4}$ (a) and $\tau=5\times10^{-5}$ (b).

with an increase of about 130% over the initial length. These results are consistent with the simulational results of Fig. 9, which show times to maximal length that bracket the experimental times, though the simulations generally achieve greater length amplification. These differences could be the result of the strong dependency in measures such as perimeter length upon the choice of initial data.

The agreement in the number of fingers is not so necessarily close for the other surface tensions which we compared. Figure 12(a) compares a single simulation with experimental data for $\tau=2\times10^{-4}$ (two experimental runs). The experimentally observed number of fingers is clearly smaller than the results from the simulation. As has been discussed before, the experiments for this control parameter displayed little finger growth [see Fig. 4(right)], making it difficult to count the fingers. This could easily lead to an underestimation of the number of fingers. In contrast the initial data for the simulation were chosen to well excite a large band of high modes and yield strong patterning. Figure 12(b) is a similar comparison for $\tau=5\times10^{-5}$. As it was not possible to run the simulations for $\tau=2.5\times10^{-5}$ corresponding to the experimental results from Fig. 4, we choose to compare the data from the simulations to another experiment with $\tau=5.6\times10^{-5}$ ($V_0=8.73$ μm/s, $\eta=11.5$ Pas, and $b_0=0.3$ mm). For this case only one experimental run has been performed. Note that we allowed for a small time shift of the experimental data due to the fact that the zero is not perfectly well defined as discussed before. Nevertheless the observed agreement is quite good. A very comprehensive (and computationally expensive) study of the effect of initial data was only performed for the case $\tau=8.4\times10^{-5}$, and it seems quite possible that such a study would reveal better agreement for the first case, $\tau=2\times10^{-4}$.

V. LIFTING FORCE

In this section we discuss how the fingering pattern affects the lifting force. Several recent studies have examined the influence of either cavitation or fingering on the lifting force during the debonding of Newtonian liquids. Tirumkudulu *et al.*[15] studied the influence of cavitation, Poivet *et al.*[14] the influence of cavitation and fingering, and Derks *et al.*[10] the influence of fingering on the lifting force. Whereas all these studies seem to agree that cavitation alters the lifting force, the effect of fingering remains unclear. Poivet *et al.* worked with a highly viscous silicon oil and report a decrease of the lifting force whereas Derks *et al.* worked with a less viscous oil and could not confirm this result within their experimental resolution.

Here we summarize some of the observations already made in Derks *et al.*[10] and discuss in more detail the relation between the measured lifting force and the observed patterns. Furthermore, the results of the numerical simulations will allow us to evaluate the parameters determining the influence of fingering on the lifting force and will give a possible explanation for the disagreement between the different observations made so far.[10,14]

A. From experiments

First consider Fig. 13, which shows the experimentally determined (dimensional) force as a function of t'. (Some of these data have already appeared in Derks *et al.* though in a different form.) We choose here to represent the absolute values of the force as a function of t' as this allows a direct comparison to the observations of the fingering patterns. The solid curves represent the theoretical prediction for Newtonian fluids, assuming a stable circular interface [Eq. (10)]. An important consideration when pairing the experimental data to the theoretical prediction is the influence of the apparatus on the force, which is not taken into account in Eq. (10).

This effect has been studied by Francis and Horn[16] and we have characterized the influence of the apparatus we use on our data in Derks *et al.*[10] For our experimental conditions this effect is most pronounced for the thinnest layer and at small t' where one can easily distinguish an overshoot of the force in the beginning of the experiment (Fig. 13). For the two other experiments no significant effect of the apparatus can be observed. Derks *et al.*[10] have shown that for our experimental conditions from $t'=0.5$ onward the influence of

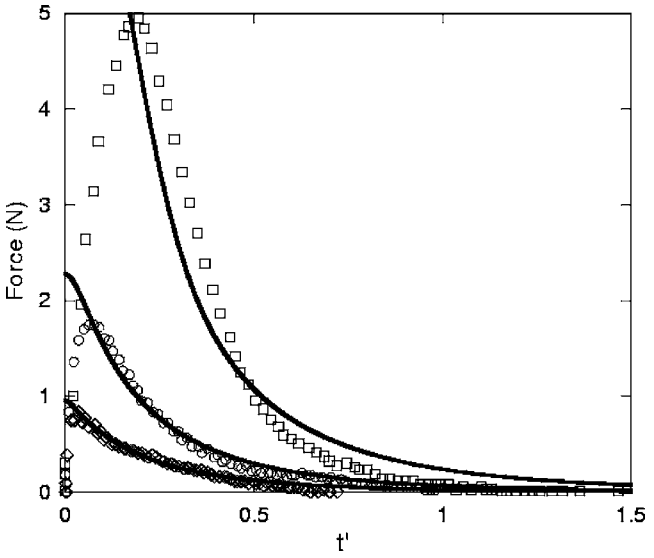

FIG. 13. Experimental results for the dimensional force as a function of $t'=t(V_0/b_0)$. Same experiments as for Fig. 4: one silicon oil (η=92 Pas), but different initial plate spacings b_0=0.2 mm (□), b_0=0.3 mm (○), and b_0 =0.4 mm (◇), leading to $\tau=2.5\times10^{-5}, 8.4\times10^{-5}$, and 2×10^{-4}, respectively. The solid line represents the theoretical prediction from Eq. (11) assuming a circular interface.

the apparatus is negligible even for the thinnest layer. As the effect of fingering is expected to become important at larger times for simplicity we will not take the apparatus into account here.

One sees immediately that for the experiments with $\tau=2\times10^{-4}$ and $\tau=8.4\times10^{-5}$ we cannot, within our experimental resolution of 0.04 *N*, see any influence from the fingering. Indeed, when comparing the fingering pattern (Fig. 6) for these two cases one sees very little deviation from a contracting circle for $\tau=2\times10^{-4}$, while for $\tau=8.4\times10^{-5}$ there is more deviation from the circular interface through finger growth. This growth sets in at about $t'=0.5$ and the deviation from the circular interface is maximal at about $t'=1.5$, after which the pattern contracts toward a circle [see Fig. 4(right)]. As the force decreases as $1/b^5$ and thus as $1/(1+t')^5$, it is already quite small at $t'=0.5$ and below the experimental resolution by $t'=1.5$. So this could explain in this case also why we do not observe an influence of the fingering on the lifting force.

For the experiment of $\tau=2.5\times10^{-5}$ one observes stronger finger growth which has a maximal deviation from the circular interface at $t'=0.5$–1.0, where in this case the force is still rather large and one observes effectively a small deviation from the theoretical prediction from $t'=0.5$ onward. In Derks *et al.*[10] it has been discussed that this might be due to a thin layer of fluid left behind on the plates as the bubble contracts. Here we measured the surface area of the bubble as a function of time. From this we can calculate an average radius and compare the results to the theoretical prediction without loss of volume (not shown here). It turns out that effectively there is some loss of volume during the experiment, however, the influence of this loss on the force can only be seen at a quite late stage of the debonding ($t'>4$), where the force is already so small, that once again it is not resolvable within our experimental resolution. The small deviation observed in this case, might thus be attributed to fingering.

In summary, we see within our experimental resolution no influence of fingering on the lifting force for the higher initial plate spacings. This might be connected to the fact that the finger growth is in this case rather small and furthermore sets in at times where the lifting force is already quite small. For the smallest initial plate spacing the finger growth is more pronounced and a small deviation of the lifting force from the circular result is observed, and is perhaps related to fingering.

B. From simulations

Figure 14(a) shows the calculated lifting force for the simulations shown in Fig. 8 (with $\tau=8.4\times10^{-5}$) and for the reference circular bubble [same line coding as in Figs. 9(a) and 9(b)]. Unlike the experiment, there is no compliance of

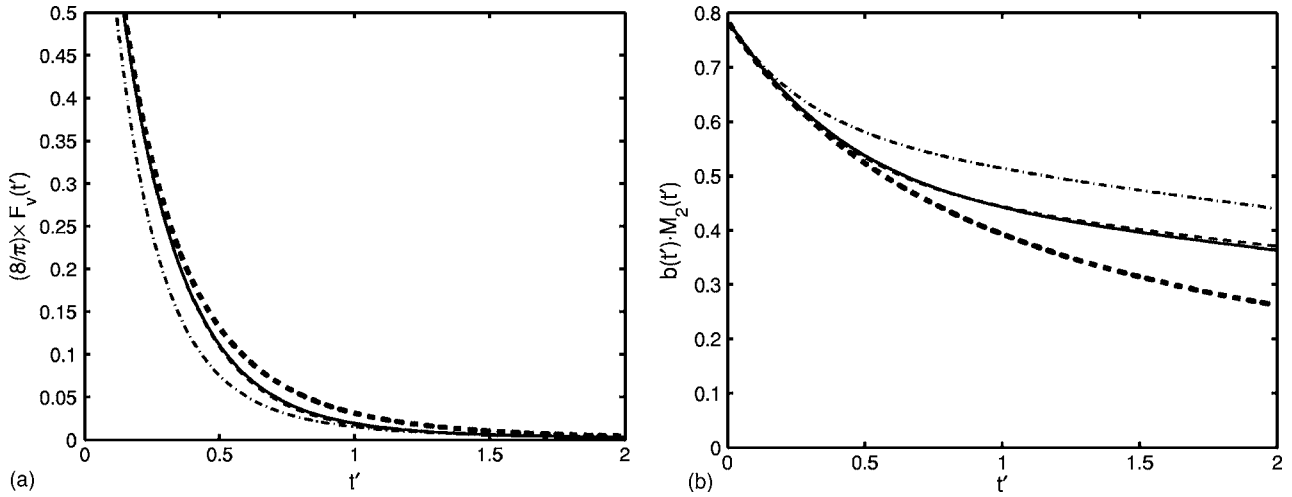

FIG. 14. (a) The viscous lifting force $F_v(t')$ for the runs shown in Fig. 8 (with $\tau=8.4\times10^{-5}$) and for the contracting circle. F_v has been multiplied by $8/\pi$ so that each curve is close to unity at $t'=0$, and the same curve coding is used as in Fig. 9 (case A curve is solid, case B is dotted, case C is dot-dashed, contracting circle is thick dashed). (b) Plots of $b(t')M_2(t')$ for the same cases and with the same coding as above.

the apparatus to contend with, and the lifting force decreases rapidly and monotonically from $t'=0$ in all cases, with simulation and the circular case clearly separated but agreeing closely. Having normalized the lifting force (by multiplication by $8/\pi$ so that each curve is close to unity at $t'=0$) we see that by $t'=1$ the force has dropped to only 5% of its initial value, while the cross-sectional area of the bubble has decreased to only $1/2$ of its initial value. Consultation with Fig. 8 also shows that at $t'=1$ the fingering pattern is already well developed. As discussed above, it is this feature of rapidly decreasing force that makes the effect of fingering instabilities on it particularly difficult to quantify in experiment.

On the time interval shown, F_v measured from the simulations lies below that of the circle in all cases, with increased ramification of the interface giving apparently decreased lifting force. This can be understood heuristically from Eq. (8):

$$F_v = \frac{1}{2b^3}\frac{d}{dt'}[b(t')M_2(t')].$$

Figure 14(b) shows $b(t')M_2(t')$ for the three simulations, and the circular case. For patterns centered at the origin, as these are, the unnormalized second moment M_2 emphasizes the mass of the pattern away from the origin. We observe generally a decrease in $b(t)M_2(t)$ as the domain shrinks, but the development of fingering patterns leaves relatively more mass away from the origin. This yields greater unnormalized second moments, with the temporal persistence of the patterns reducing the slopes of $b(t)M_2(t)$ relative to the circular case, as the figure shows. The consequent decrease in lifting force is increased by greater ramification of the pattern. At times beyond what have been plotted, when the lifting force is extremely small, both pattern and lifting force begin to converge toward the circular case.

Finally, we examine the effect of varying surface tension on the production of lifting force. Recall that in our nondimensionalization of the problem the effective surface tension enters the dominating viscous lifting force only indirectly through the evolution of $M_2(t')$. Hence we expect that as reducing surface tension will both increase interface ramification and the temporal persistence of the pattern, the lifting force will be reduced. This expectation is verified by Fig. 15, which shows $F_v(t)$ for three characteristic simulations at various values of τ (that shown in Fig. 3, case C of Fig. 8, and another simulation for $\tau=2\times10^{-4}$ with a large band of excited modes). In a manner consistent with the results above at a single τ, where changes in initial data increased the depth of fingering and lowered the lifting forces, we find that increases in interface ramification by decreasing surface tension lead also to generally lowered lifting force.

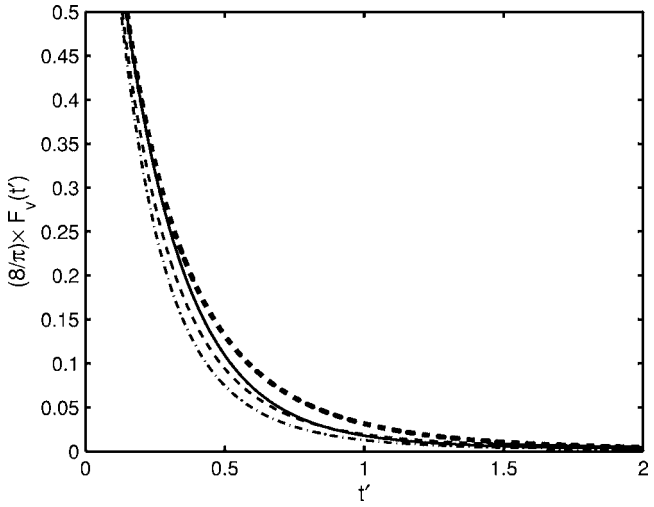

FIG. 15. A comparison of the viscous lifting force as the effective surface tension τ is changed. The simulations are for $\tau=2\times10^{-4}$ (solid curve), $\tau=8.4\times10^{-5}$ (dashed curve), and $\tau=5\times10^{-5}$ (dot-dashed curve).

Discussion

In conclusion, the fact that in the experiments we see little if any effect of the fingering on the force is not a universal result, but is due rather to the fact that the perimeter does not grow so strongly in our experiments and hence the effect on the force is rather small. This may explain also why other experimental groups observed a slight decrease of the lifting force due to fingering.

VI. CONCLUSION

In the present paper we studied the debonding of two circular plates bonded together by a Newtonian liquid, comparing experimental results with numerical simulations. In particular, we studied the evolution of the interface of the originally circular bubble confined between the two plates when lifting the upper plate, and related the observed pattern to the lifting force.

Experimentally, we characterized the fingering patterns in terms of the number of fingers and the amplitude of these growing fingers through the perimeter length. Once experimental conditions are fixed, we showed that the number of fingers is solely determined by the dimensionless control parameter τ. Once this parameter is known the initial number of fingers as well as the decrease of the number of fingers with time is determined. This decrease seems to be exponential in time. Experimental results are in good agreement with results from numerical simulations using the formalism of the Saffman–Taylor[29] instability adapted to the special geometry of the stretch flow.

We found that the extent of finger growth, i.e., perimeter length, is a less robust parameter and depends not only on the control parameter but also on initial conditions. The influence of the initial conditions was studied intensively in numerical simulations where the initial number of modes and the amplitude of the perturbation of the initial interface were tuned independently. However, in the experimental situation it is difficult to determine the exact parameters governing the initial fluctuations of the air–fluid interface. We suspect that not only fluid viscosity and initial plate spacing determine the fluctuations of the interface, but also that more subtle effects, such as the way the sample is prepared, might be influential.

Numerical simulations reveal that the influence of fingering on the lifting force depends on the extent of finger growth. The higher the amplitude of the fingers, the stronger the influence on the lifting force. In this case the lifting force is observed to decrease relative to a contracting circle. These results explain also why in the experiments very little deviation from the circular case is observed: In the experiments, the extent of finger growth is rather small and its effect on the lifting force is lost within our experimental resolution. Furthermore, this finding may explain why different groups have found contradictory results concerning the influence of fingering on the lifting force. It depends not only on the control parameter but also on the initial conditions.

In summary we have studied the fully nonlinear evolution of the fingering pattern, taking both the number of fingers and the amplitude of the fingering growth into account, and relating the fingering pattern to the observed lifting force. The results obtained here for simple Newtonian fluids might be a starting point for the study of the debonding of more complex visco-elastic materials and commercial adhesives.

ACKNOWLEDGMENTS

A.L. and D.D. are indebted to Daniel Bonn and Martine Ben Amar for useful discussions. Most of the experiments presented in this paper were performed in the laboratory of our collaborator Daniel Bonn. M.J.S. thanks Krzystof Wlodarski for useful conversations and assistance, and acknowledges the support of DOE Grant No. DE-FG02-88ER25053 and NSF Grant No. DMS-9980069.

[1] K. Autumn and A. M. Peattie, "Mechanisms of adhesion in geckos," Integr. Comp. Biol. **42**, 1091 (2002).
[2] W. Federle, W. Baumgartner, and B. Holldobler, "Biomechanics of ant adhesive pads: Frictional forces are rate- and temperature-dependent," J. Exp. Biol. **207**, 67 (2004).
[3] A. Zosel, "Adhesion and tack of polymers: Influence of mechanical properties and surface tensions," Colloid Polym. Sci. **263**, 541 (1985).
[4] H. Lakrout, P. Sergot, and C. Creton, "Direct observation of cavitation and fibrilation in a probe tack experiment on model acrylic pressure-sensitive-adhesives," J. Adhes. **69**, 307 (1999).
[5] A. J. Crosby, K. R. Shull, H. Lakrout, and C. Creton, "Deformation modes of adhesively bonded elastic layers," J. Appl. Phys. **88**, 2956 (2000).
[6] C. Creton, J. C. Hooker, and K. R. Shull, "Bulk and interfacial contributions to the debonding mechanisms of soft adhesives: Extension to large strains," Langmuir **17**, 4948 (2001).
[7] K. R. Shull, C. M. Flanigan, and A. J. Crosby, "Fingering instabilities of confined elastic layers in tension," Phys. Rev. Lett. **84**, 3057 (2000).
[8] J. Bohr, S. Brunak, and T. Norretranders, "Viscous trees and Voronoi-structure formation in expanding systems," Europhys. Lett. **25**, 245 (1994).
[9] H. Van Damme, S. Mansoutre, P. Colombet, C. Lesaffre, and D. Picart, "Pastes: lubricated and cohesive granular media," C. R. Phys. **3**, 229 (2002).
[10] D. Derks, A. Lindner, C. Creton, and D. Bonn, "Cohesive failure of thin layers of soft model adhesives under tension," J. Appl. Phys. **93**, 1557 (2003).
[11] R. D. Welsh, M.Sc. thesis, supervised by J. Bico and G. H. McKinley, MIT, Cambridge, MA (2001).
[12] S. H. Spiegelberg and G. H. McKinley, "Stress relaxation and elastic decohesion of visco-elastic polymer solutions in extensional flow," J. Non-Newtonian Fluid Mech. **67**, 49 (1996).
[13] A. Ghatak and M. K. Chaudhury, "Adhesion-induced instability patterns in thin confined elastic films," Langmuir **19**, 2621 (2003).
[14] S. Poivet, F. Nallet, C. Gay, and P. Fabre, "Cavitation induced force transition in confined viscous liquid under traction," Europhys. Lett. **62**, 244 (2003).
[15] M. Tirumkudulu, W. B. Russel, and T. J. Huang, "On the measurement of "tack" for adhesives," Phys. Fluids **15**, 1588 (2003).
[16] B. A. Francis and R. G. Horn, "Apparatus-specific analysis of fluid adhesion measurements," J. Appl. Phys. **89**, 4167 (2001).
[17] M. Ben Amar and D. Bonn, "Fingering instabilities in adhesive failure," Physica D (to be published).
[18] A. Lipshat, B. Meerson, and P. V. Sasorov, "Anomalous scaling in locally conserved coarsening of fractal clusters," Phys. Rev. E **65**, 050501(R) (2002).
[19] E. Sharon, M. Moore, W. McCormick, and H. Swinney, "Coarsening of fractal viscous fingering patterns," Phys. Rev. Lett. **91**, 205504 (2003).
[20] M. J. Shelley, F.-R. Tian, and K. Wlodarski, "Hele-Shaw flow and pattern formation in a time-dependent gap," Nonlinearity **10**, 1471 (1997).
[21] C.-W. Park and G. Homsy, "Two-phase displacement in Hele-Shaw cells: Theory," J. Fluid Mech. **139**, 291 (1984).
[22] D. Reinelt and P. Saffman, "The penetration of a finger into a viscous fluid in a channel and tube," SIAM (Soc. Ind. Appl. Math.) J. Sci. Stat. Comput. **6**, 542 (1985).
[23] D. Reinelt, "Interfacial conditions for two-phase displacement in Hele-Shaw cells," J. Fluid Mech. **177**, 67 (1987).
[24] D. Reinelt, "The effect of thin film variations and transverse curvature on the shape of fingers in a Hele-Shaw cell," J. Fluid Mech. **285**, 303 (1995).
[25] L. Paterson, "Radial fingering in a Hele-Shaw cell," J. Fluid Mech. **133**, 513 (1981).
[26] T. Hou, J. Lowengrub, and M. J. Shelley, "Removing the stiffness from interfacial flows with surface tension," J. Comput. Phys. **114**, 312 (1994).
[27] T. Hou, J. Lowengrub, and M. J. Shelley, "Boundary integral methods for multicomponent fluids and multiphase materials," J. Comput. Phys. **169**, 302 (2001).
[28] R. Almgren, "Singularity formation in Hele-Shaw bubbles," Phys. Fluids **8**, 344 (1996).
[29] P. G. Saffman and G. I. Taylor, "The penetration of a fluid in a porous media or Hele-Shaw cell, containing a more viscous liquid," Proc. R. Soc. London, Ser. A **245**, 312 (1958).